Int. J. Electrochem. Sci., 12 **(2017)** 4928 – 4939, doi: 10.20964/2017.06.38

International Journal of ELECTROCHEMICAL SCIENCE
www.electrochemsci.org

Short Communication

Electrochemical Reactivation of AISI 409 Ferritic Stainless Steel Sheet Welded by Laser Process with application in aeronautical

M.C. Ramírez-López[2], *L.A. Falcón-Franco*[2], *F.F. Curiel-López*[2], *P.Zambrano R*[1]., *J.A. Cabral-Miramontes*[1], *C. Gaona-Tiburcio*[1], [*]*F.Almeraya-Calderón*[1].

[1] Universidad Autónoma de Nuevo León, UANL. Facultad de Ingeniería Mecánica y Eléctrica, FIME Centro de Investigación e Innovación en Ingeniería Aeronáutica, CIIIA, Av. Universidad S/N. Ciudad Universitaria. 66455 San Nicolás de los Garza, Nuevo León, México.
[2] Universidad Autónoma de Coahuila. Facultad de Metalurgia, Carretera 57, Monclova, Coahuila.
[*]E-mail: falmeraya.uanl.ciiia@gmail.com

Received: 22 February 2017 / *Accepted:* 11 April 2017 / *Published:* 12 May 2017

The susceptibility to sensitization in 409 ferritic stainless steel (FSS) weldments was studied, by means of double loop electrochemical potentiokinetic reactivation test (DL-EPR). After the electrochemical test, the microstructure was analyzed by scanning electron microscopy (SEM) and the presence of elements with dispersive energy of X-rays (EDS), with the X-ray diffraction (XRD) technique they were identified present phases in different welds. Microhardness profiles were employed to evaluate the mechanical properties. With the aim of analyze the effect on the degree of sensitization to welding processes and the base material, a methodological analysis of gas metal arc welding GMAW, gas tungsten arc welding GTAW and LASER welding process was performed. The LASER process generated the highest ratio between the reactivation (Ir) and activation (Ia) current, despite it caused less microstructural change. The higher ratio Ir/Ia is attributed to the lack of penetration in the butt join, showing crevice corrosion.

Keywords: 409 Ferritic stainless steel, DL-EPR, GMAW, GTAW, LASER.

1. INTRODUCTION

A stainless steel is base iron, with proportion chromium content above 10% [1-2], contact with the environment, a passive interface CrO_3 is generated, giving the specific property of corrosion resistance and inhibiting the oxidation-reduction process. Stainless steels are classified according to the present phase in, martensitic, austenitic, duplex and ferritic, FSS are defined with a chromium content between 10.5 and 30%. FSS have the alpha phase of iron, which is stable below 950°C and are

characterized by a crystal structure body centered cubic (BCC) [2-3]. In this study, 409 FSS demined of low chromium content between 11 and 12% was studied [4]. These stainless steel are used in various industries like automotive catalysts, furnace parts with chemical processing, heat exchangers, electrical and heat storage containers [5]. In the aircraft industry it is applicable for various components in the pylon structures, such as fasteners engine to the wing and stringers [6-7] and parts of secondary structures.

The gas metal arc welding process (GMAW) is a versatile process that uses a solid electrode wire feed continuously through a welding torch. The arc between the electrode wire and workpiece is created and a plasma forms due the interaction of arc with the argon. This process has limited applications in the aviation industry due to the large effect of microstructure in the heat affected zone (HAZ).

LASER welding is a relatively new process and microstructural changes due the heat effects is lower than other processes [8, 9]. The weldments performed with filler material [10], present poor corrosion resistance due the galvanic effects generated in the microstructure by thermal effects. On the other hand, laser process present a less microestructural changes, therefore, the corrosion rate is less, all this condition can help in the reduction of thermic and residual stress [11-12]. However, the 409 ferritic stainless steel under any welding process, becomes more vulnerable to sensitization or intergranular corrosion. Chromium carbides precipitate in the grain boundaries due to thermal exposure. With induced thermal process, near areas of grain boundary are chromium depleted, thus inevitably corrosion process develops when exposed to aggressive environment. The DL-EPR technique has been proven to be a reliable test in assessing the level of sensitization in different stainless steels [13]. The DL-EPR test measures the charge associated with the corrosion of depleted in chromium areas. These particles in a sensitized microstructure, are located in the grain boundaries [3].

Researchers have been supported the foundation of this work as, M.C. Li [14] who experiment with electrochemical tests, simulating operation conditions in 409 FSS weld. M.C. Li found that the atmosphere sulfides were deposited at the interface of the material; they inhibited the growth of the oxide layer and reducing the passive current density; A.K. Lakshminarayanan [15] analyzed the friction stir welding process in 409M FSS through DL-EPR; in this study, the fusion zone has the higher sensitization resistance, it´s attributed to the fine grain size and less heat input; Subsequently, A.K. Lakshminarayanan [5] analyzed the susceptibility of 409M FSS after gas tungsten arc welding process, friction stir, LASER and electron beam welding. A.K. Lakshminarayanan found that friction stir welding is less susceptible to sensitization. Tae Jun Parka [16] analyzed an Al-S coating in joint of 409L FSS by GTAW process, finding titanium precipitates in the weld zone. Tae Jun Parka attributed the hardness reached to TiN precipitates in fusion zone, finding vulnerable zones in the welding area. Other researches, M.A. García-Rentería, et al [17] used the DL-EPR technique to assess the susceptibility to intergranular corrosion in duplex stainless steels with austenitic and ferritic matrix, magnetic fields in welding process was applied; N. Ortiz, et al [13] analyzed and correlated the degree of sensitization through a non-destructive technique calling thermoelectric potential, finding current values of activation current between 10^{-2} to 10^{-1} in anodic loop. Cabral Miramontes J. A, et al [18] performed the electrochemical characterization of 409Nb FSS adding amounts of boron into hydrogen atmosphere and corrosion resistance was analyzed, specimens with addition of boron were more prone

to corrosion, it is was attributed to the presence of chromium carbides (Cr_3C_2), they generating galvanic zones with boron added, this study hope found chromium carbides, who will have corrosion effect in corrosion behavior.

Some of the current applications of the Laser welds in stainless steel are in automotive and aeronautical industry, like the vane of the missiles Patriot and other accessories of aircraft. This vane consists of an investment cast frame of stainless steel over which sheet metal of the same composition is welded with laser. The process of laser welding is an important technology to use, due to its low thermal input which allows to substitute with advantage other welding techniques currently applied, hence the interest to characterize this welding processes in stainless steel Therefore, the objective of this study is to find advantages and disadvantages between the microstructural effects and the electrochemical behavior of 409 FSS welded by GMAW, GTAW and LASER process.

2. EXPERIMENTAL PROCEDURE.

2.1 Base Material.

Type 409 ferritic stainless steel with a thickness of 1.6 mm was used in this work. Experimental chemical composition determinate by X-ray fluorescence technique is showed in Table 1.

Table 1. Chemical composition of 409 FSS (% wt).

Material	Fe	Cr	Si	Mn	Ti	Ni	V	P	Cu	Mo
SS409	88.01	10.73	0.34	0.34	0.24	0.14	0.05	0.025	0.11	0.016

2.2 Welding process.

Samples of 150mm length and 75mm wide were cut and prepared according to AWS D1.9 standard [19] to be weld.

2.3 Microstructural characterization of joint.

After welding, the samples were cut transversally to the welding direction. Then were mounted in bakelite to isolate their conductivity. The cross section were grinded with emery paper from 80 to 4000 ppm. Next mounting, the weldments were polished with diamond paste of 6, 3 and 1μm by mirror finish [20]. The specimens were etched by one minute to Kalling´s reagent and the microstructure was revealed [21], the surface was cleaned with C_3H_6O and then analyzed in a Carl Zeiss Axion Vert.A1^{TM} optical microscope to 5X.

2.4 Electrochemical test: DL-EPR Technique.

The specimens of 20x20x1.6mm were cut transversely, which were attached to a 16 gauge copper wire, ensuring its electrical continuity. These samples were mounted in epoxy resin and after 12 hours of curing were grinded with emery paper from 80 to 1200 ppm before the test, as indicated by the ASTM G1 standard [20]. The electrochemical characterization was performed using the DL-EPR technique as shown in the literature [8], with base in ASTM G108 standard [3]. A polarization of ± 600 mV was used respect to open circuit potential (OCP), with a maximum of three minutes after performing grinded with emery paper of 1200 ppm, the specimen was subjected to cathodic passivation for three minutes, the scan speed was 200 mV/min., 0.1 M H_2SO_4, 0.01 M KSCN, 0.4 M Na_2SO_4 was used as electrolyte environment [2]. The test was development in atmospheric environment and a pH of 1. A Typical three electrodes cell was used in electrochemical test, satured electrode of calomel as reference electrode, graphite as auxiliary electrode and the weld as working electrode was applied.

The areas exposed in the working electrode of the 409 FSS specimens in different welding processes were 11 mm^2 for base material, LASER 14 mm^2, 10 mm^2 in GTAW and GMAW 17 mm^2. After DL-EPR test, the samples were observed in secondary electrons in a scanning electron microscopy equipped with EDS analyzer, the specimens was prepare according to ASTM E3 standard [22]. Searching chromium carbides in grain boundary and change of phases, a specimen was exposed to Energy dispersive analysis of X-ray technique.

2.5 Mechanical test.

The mechanical properties of the specimens were evaluated by microhardness profiles, Figure 5 shows the diagonal profile for GMA welding, the profile in the GTAW and LASER was performed longitudinally through the specimen, in all cases, 2θ indentations were realized with a 0.5 mm separation between each center. Microhardness measurement was performed on the base material, HAZ and weld metal, with a load of 100g for 15 seconds, according to the ASTM E92 standard [23].

2.6 X-ray diffraction.

The test specimens were cut in centers of weld beat transversely by diffraction analyses, with a height of 2 mm, the specimens were grinded with emery paper, and then polished with diamond paste 6μm. Using X-ray radiation from a Cu anode (45 kV, 40 mA, View the MathML source). The X-ray diffraction patterns were collected in continuous scanning mode with interval of 0.02° at a speed of 3°/min. for an angle to 2θ, from 20° to 140°.

3. RESULTS AND DISCUSSION.

3.1 Macrostructural profile.

Figure 1 shows the macrostructural profile of GMAW, GTAW and LASER welds to 5X. Figure 1a shows the microstructure of the GMA weldment, in can be appreciated that the welding variables employed melted both the top and the bottom plates. The weld reinforcement is adequate and the weld toe does not show the presence of any crack. Notwithstanding, the weld pool shows an epitaxial solidification pattern, which it is characteristic of fusion welding processes. On the other hand, at the top of the weld, grain refinement is observed; this is attributed to the presence of Ti in the filler metal. The bottom plate shows grain growth in the heat affected zone as a consequence of the heat input imposed by the arc energy.

Figure 1b shows GTAW welding, area with grain refinement in the heat affected zone, the columnar growth can be appreciate in all welding toward the power source. Damage lamination induced in the manufacture process is observed in the center of the plate. Figure 1c shows the laser welding with a penetration of 37%. It is well know that the heat input in lase process cause a narrow heat affected zone and little distortion of the workpiece [24], this can be seen in figure 1d, were despite the presence of columnar grains, the wide and length are equal to those observed in the base metal.

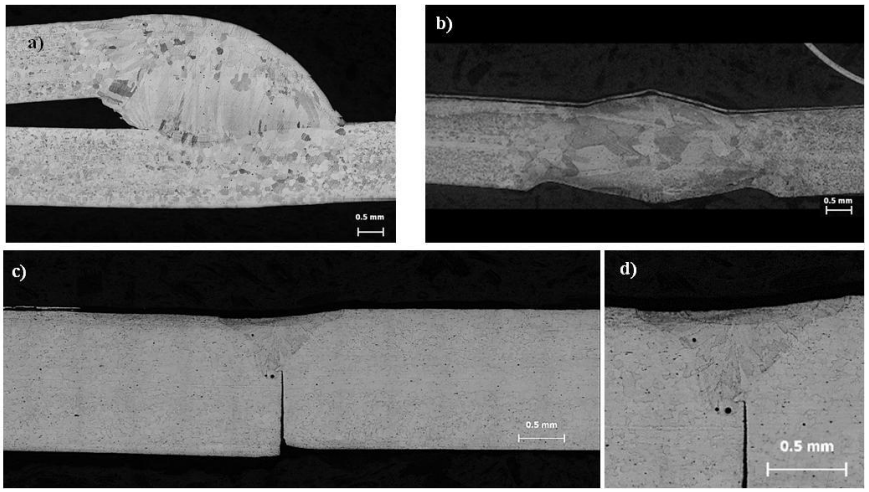

Figure 1. Macrostructural profile a) GMAW, b) GTAW, c) and d) LASER welds.

3.2 Electrochemical characterization.

Graphs obtained in DL-EPR technique are showed in Figure 2, base metal (BM, black), GMAW (red), GTAW (blue) and LASER (green) are define, activation current (Ia) is appreciate in the highest pick of anodic loop during the activation, reactivation current (Ir) is the highest pick in anodic loop during reactivation process [17]. LASER weld present more high activation and reactivation current respect with each welds and base metal. The change in the activation and reactivation loops observed in the LASER weld is attributed to the lack of penetration. The specimen has zones without fusion and the corrosion process kinetic in this specimen involucre a crevice corrosion process.

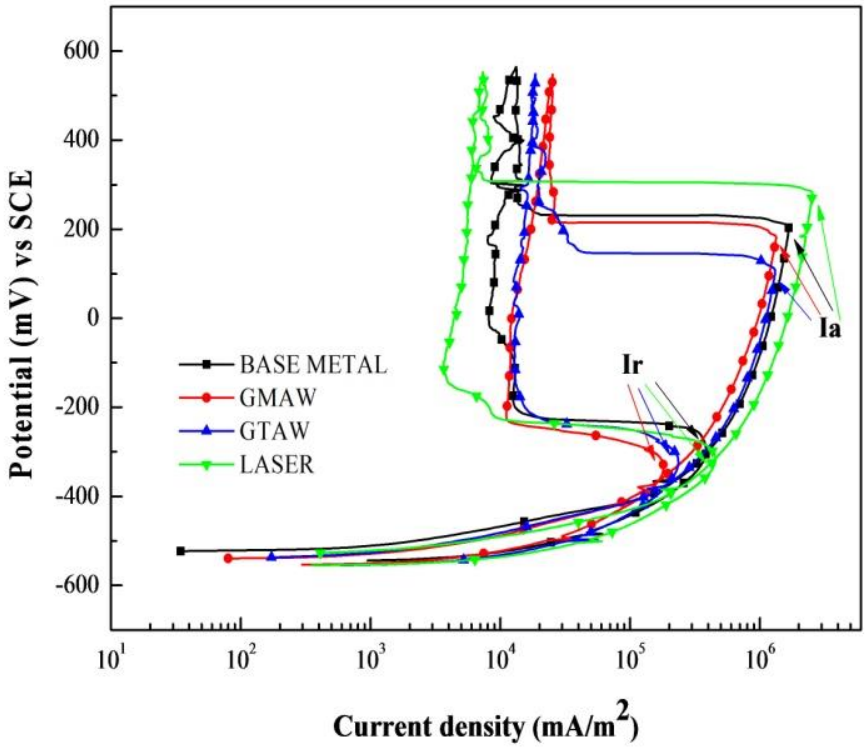

Figure 2. Double loop electrochemical potentiokinetic reactivation (DL-EPR) technique of the 409 FSS and welds

The crevice corrosion process is like localized corrosion occurring in restricted flow areas, where the metal surface is in contact with a small volume of deposit, either by design or wear during service [24]. Crevice corrosion occurs due to limited mass transfer for diffusion from the interior of the gap to the environment, local environment presents changes in the gap with more aggressive conditions [25-26]. In DL-EPR testing, passivation of specimen is looking, being in this state, the conditions become more aggressive in the area without fusion due to the less oxygen, causing the breakdown of passivation and starting active dissolution, which increases the current values for LASER welding. Table 2 shows the values obtained in the activation and reactivation current and the degree of sensitization (DOS) ratio between Ir/Ia of each weld.

Tatıs Campos Scalise, et al [27] studied the intergranular corrosion resistance of the AISI 409 ferritic stainless steel, after annealing at 300, 500, and 700 ^{o}C for 2, 4, and 6 h. The authors found similar behavior of this work, the values of DOS exposed in the annealing specimens are around 20 to 38%, this fact shows that the weldments performed in the present study, suffered annealing during the weld process. This aspect diminishes the DOS in the in the FSS. Jin Ho et al [28], found values of DOS around 2 to 4% in a low carbon ferritic stainless steel.

Table 1. Parameters of electrochemical DL-EPR.

Specimen	Ia (mA/cm^2)	Ir (mA/cm^2)	Ia/Ir %
BM	167.31	38.56	23.05
GMAW	133.66	18.12	13.56
GTAW	131.77	23.56	17.88
LASER	254.6	45.49	17.87

The relationship between reactivation and activation current (Ir/Ia) showed in Table 2, comparing these results with images of the specimen after DL-EPR test through SEM, the effect is observed. Into welding process, heat treatment was generated in the specimen, improving corrosion resistance and decreasing degree of sensitization. The base metal shows the highest degree of sensitization with a value of 23.05%, while GMAW samples have the less effect in degree of sensitization, due to the compensation in the areas, the anode and cathode region between the weld and base material had similar size, an electrochemical balance was created, reducing the corrosion process.

GTAW and LASER specimens have higher DOS values in formed cell, with degrees of 17.88% for GTAW and 17.87% in LASER, these processes are more active than GMAW.

In other studies [27], lower values of DOS have been found. Its seems that the material employed in this study has suffered microstructural changes due thermal history during its fabrication.

In Figure 3, the images obtained by SEM after the DL-EPR test are showed. Susceptibility to intergranular corrosion in base metal is shown in Figure 3a at 250X. The microstructure of the base material after DL-EPR test shown areas corresponding to the chromium carbides in red box, it is conclusive for EDS analysis in Figure 3b; Figure 3c) corresponding to the specimen surface of GMAW process at 250x, titanium precipitates were found in 88.74% of composition by EDS analysis in weld area (Figure 3d). Ti precipitates at grain boundaries, chromium carbides and chromium depletion zones near the grain boundary forming an galvanic effect in the microstructure, it is shows in Figure 3e for the GTAW welding process at 500X, it shows chromium carbides (Cr_3C_2) in grain boundaries by EDS, its defined by red line, Figure 3f shows the EDS of GTAW, Cr_3C_2 were founded in grain boundary.

LASER is a welding process without filler metal and the microstructural effect is less than the GMAW process, however, the degree of sensitization in GTAW is 14.32% higher than the GMAW, this is attributed to the area ratio between base material and weld, weld zone acts as anode zone and, difference between areas accelerates the corrosion process. Figure 3g and 5h shows the LASER specimens after DL-EPR test, with currents in degree of 10^2 for electrochemical test, Figure 3g shows the surface results in fusion line by LASER specimen at 500X, residual sulfides of the environment was showed in red rectangle, residual sulfides are primarily responsible generalize corrosion for this specimen. Figure 3h at 1000X shown the chromium carbide precipitates in the fusion line. For this specimen, the crevice corrosion process occurs between the partially fused zone and the specimen, due to the various corrosion processes present, the DOS obtained by DL-EPR test in LASER welding cannot be attributed entirely for intergranular corrosion.

a)

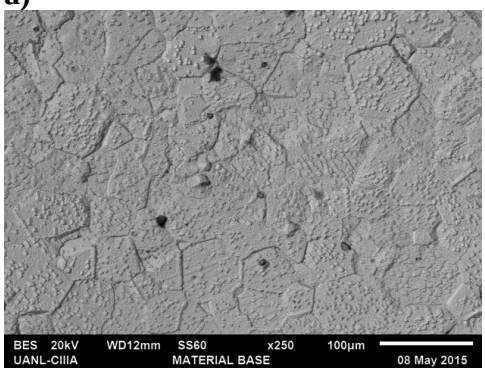

b)

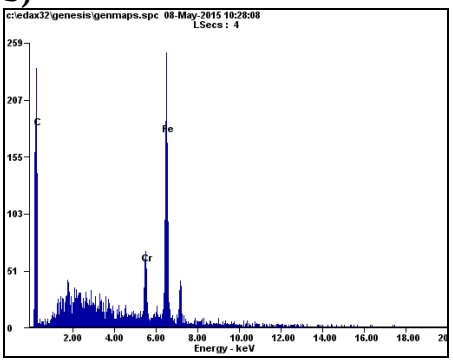

Element	*Wt%*	*At%*
CK	51.67	83.11
CrK	06.84	02.54
FeK	41.49	14.35
Matrix	Correction	ZAF

c)

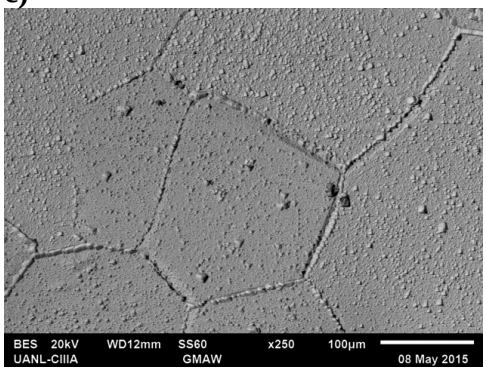

d)

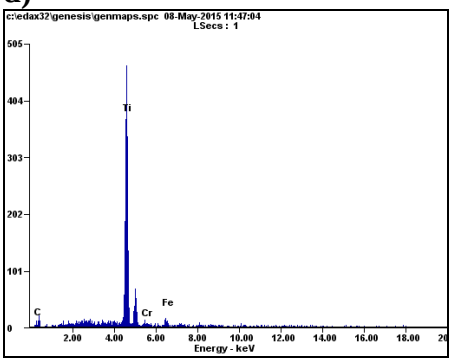

Element	*Wt%*	*At%*
CK	02.68	09.99
TiK	88.74	83.00
CrK	02.15	01.85
FeK	06.43	05.16
Matrix	Correction	ZAF

e)

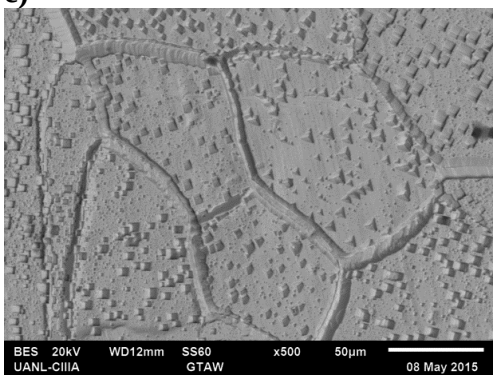

f)

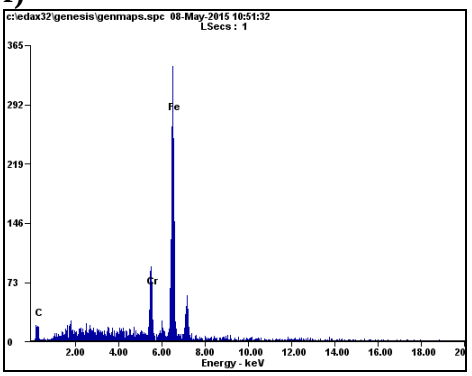

Element	*Wt%*	*At%*
CK	10.01	33.87
CrK	11.75	09.19
FeK	78.24	56.94
Matrix	Correction	ZAF

g)

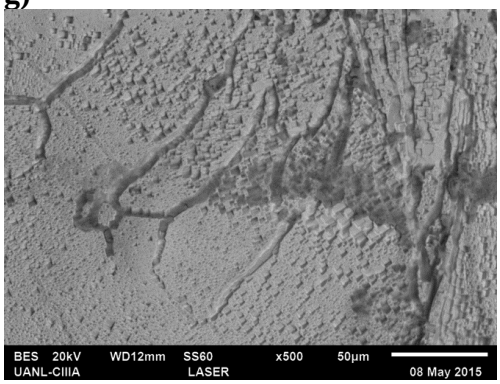

h)

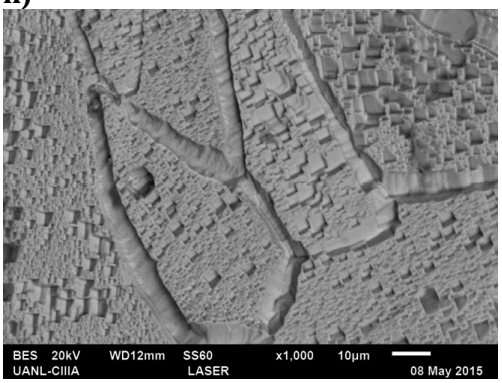

Figure 3. SEM microstructure analysis of the 409 FSS and welds after DL-EPR test: a) Base metal 250X, b) EDS in base metal, c) GMAW 250X, d) EDS in GMAW, e) GTAW 500X, f) EDS in GTAW, g) LASER 500X, h) LASER 1000X.

This results can be compared whit the SEM analysis realized by Jin Ho Park, et al [28], it indicates that most of grain boundary area is occupied by 200–300 nm size of intermetallic compounds.

3.3 Microhardness profile.

The GTAW and GMAW welding showing a homogeneous microhardness profile (figure 4), values of indentations in HAZ have a slight decrease in hardness. The highest hardness peak for GMAW welding occurs in columnar growth region in the initial edge of the joint of lower leg with a value of 182.3 Vickers, the highest peak for GTAW welding is 179.4 Vickers. It can be appreciated that the highest value was obtained in the centre of the melted zone in the LASER process, reaching values of 227.2 Vickers.

M. V. Venkatesan [29], found a variation in hardness in weld metal and HAZ of the weld joints of 409M, made with three different heat inputs. It is clear that HAZ hardness (270 VHN) is higher than that of the base metal (200VHN) and this is in agreement with the presence of martensite in the HAZ.

M. Alizadeh-Sh [30] studied spot welding of AISI 430 ferritic stainless steel, the heterogeneous hardness profile of the HAZ compared to that of FZ and BM is the result of different transformations occurring in this region of the weld. The lower value of the hardness in the HTHAZ zone compared to the adjacent regions may be contributed to the grain growth and also the absence of martensite at ferrite grain boundaries.

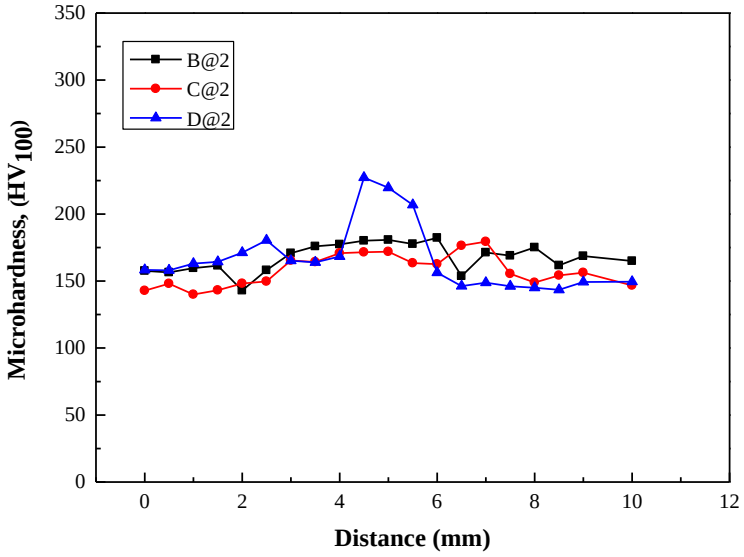

Figure 4. Microhardness profile of welds specimens.

3.4 X-Ray Diffraction.

The X-ray diffraction pattern in welded specimens shown in Figure 5. The phase present in the GMAW, GTAW and LASER welding was characterized and compared with base metal. The base metal display peaks concerning to Fe (110), Fe (200), Fe (211), Fe (220), Fe (310) and Fe (222) planes. Regarding the iron phase in the GMAW and GTAW welding process with respect to base metal, not show representative changes. Nevertheless the intensity of the planes in the LASER weld is smaller, this can due to the low heat input of the process. On the other hand, this analysis indicates that all the welding processes studied in this work don't induce the precipitation of a second phase.

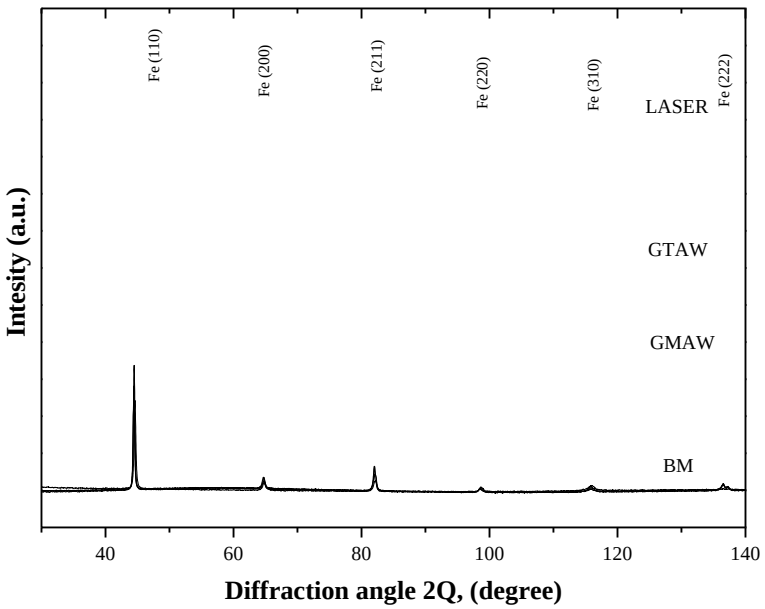

Figure 5. X-ray diffraction profile.

T. Balusamy, et al [31] studied the influence of surface mechanical attrition treatment (SMAT) on the corrosion behaviour of AISI 409 grade stainless steel in 0.6 M NaCl. They found that using 5 mm Ø 316L stainless steel (SS) balls for 15 min offers a better corrosion protective ability.

The XRD patterns of T. Balusamy, et al of untreated sample exhibits peaks pertaining to Fe (110), Fe (200) and Fe (211) planes whereas a reduction in intensity of the Fe (200) and Fe (211) planes and broadening of the peaks pertaining to all the three planes are observed for treated samples.

4. CONCLUSION

- The base material exhibits the highest degree of sensitization respect with GMAW, GTAW and LASER welding processes.
- GMAW welds has the lowest degree of sensitization, effect and/or microstructural change suffered during the welding process was favorable for sensitization resistance,

this is attributed to the major coarse grained zone due to excessive heat in the process, the ratio between generals microstructures turned more uniform than in the case of GTAW and LASER welds, it causing a process of oxidation-reduction more balanced.

- LASER welding with 37% penetration shows a similar kinetic that GTAW with degrees of sensitization of 17.87% and 17.88% respectively.
- The microstructure revealed after DL-EPR testing shows that the values obtained are not attributed only to intergranular corrosion, due transgranular corrosion are showed in each weld.
- Base metal, fine grain and coarse grain zones in GMAW present the higher value in microhardness, fusion line present a microhardness increment of 25% respect with GMAW and weld zone have 20% more hardness that GMAW.
- The analysis by X-ray diffraction shows no significant changes in the 409 FSS after welding process.

References

1. D. Benjamin and C. W. Kirkpatrick, "Properties and Selection: Stainless Steel, Tool Materials and Special-Purpose Metals", ASM International, (1980) Metals Park, OH.
2. A. J. Sedriks, "Corrosion of Stainless Steel", John Wile & Sons, Inc. (1996) New York, USA.
3. ASTM G108-07"Standard Test Method for Electrochemical Reactivation (EPR) for Detecting Sensitization of AISI Type 304 and 304L Stainless Steels", Book of ASTM Standars, ASTM (2007) West Conshohocken, PA. USA..
4. P. Lacombe, B. Baroux and G. Beranger, "Stainless Steel", Les editions de Physique Les Ulis, (1993) Francia.
5. A. K. Lakshminarayanan and V. Balasubramanian, *J. Mater. Eng. Perform.* 22-8 (2013) 2293.
6. D. Reitemeyer, V. Schultz, F. Syassen, T. Seefeld and F. Vollertsen, *Phys Procedia* 41 (2013) 106.
7. B. Cantor, H. Assender and P. Grant, "Aerospace Materials", IOP Publishing Ltd, (2001)Department of Materials-University of Oxford, UK.
8. C. L. Jenney and A. O´Brien, "Welding Hanbook", AWS (1991) Ninth Edition. Miami, FL. USA.
9. X. Gu, H. Li, L. Yang and Y. Gao, *Opt. Laser Technol.* 48 (2013) 246.
10. A. W. S. Committe, "Welding Handbook", AWS (2001) U.S.A..
11. D. Colomb, B. M. Colosimo and B. Previtali, *Opt. Laser Eng.* 51 (2013) 34.
12. B. S. Yilba, A. F. M. Ari and B. J. A. Aleem, *Opt Laser Technol*. 42 (2010) 760.
13. N. Ortiz, F. F. Curiel, V. H. López and A. Ruiz, *Corros. Sci.* 69 (2013) 236.
14. M. C. Li, H. Zhang, R. F. Huang, S. D. Wang and H. Y. Bi, *Corros. Sci.* 80 (2014) 96.
15. A. K. Lakshminarayanan and V. Balasubramanian, *Int. J. Adv. Manuf. Technol*. 59 (2012) 961.
16. T. J. Park, J. P. Kong, S. H. Uhm, I. S. Woo, J. S. Lee and C. Y. Kang, *J. Mater. Process. Technol.* 21 (20103) 415.
17. M. A. García-Rentería, F. F. Curiel-López, V. H. López-Morelos, J. A. Gonzalez-Sánchez, L. R. D. Perez and R. García-Hernandez, "Microstructural, Mechanical And Corrosion Analyses Of 2205 Duplex Stainless Steel Welded With Electromagnetic Interaction", *NACE* 2014.
18. J. A. C. Miramontes, J. D. O. B. Sánchez, C. A. P. Salas, G. K. P. Basulto, D. N. Mendoza, P. C. Z. Robledo and F. A. Calderón, *Int. J. Electrochem. Sci*. 8 (2013) 564.
19. "Sheet Metal Welding Code", AWS D 9.1, AWS (2000) 6th Edition. Doral FL. USA.
20. ASM Handbook Vol 9: Metallography and Microstructures, ASM International (2004) USA.
21. ASTM G1-03 "Practice for Preparing, Cleaning, and Evaluating Corrosion Test Specimens", Book of ASTM Standars, ASTM (2011) West Conshohocken, PA. USA.

22. ASTM E3-11"Standar Practice for Preparation of Metallographic Specimens", Book of ASTM Standars, ASTM (2011) West Conshohocken, PA. USA.
23. ASTM E 92 "Test Method for Vickers Hardness for Metallic Materials", Book of ASTM Standars, ASTM (2005) West Conshohocken, PA. USA.
24. C. Gaona Tiburcio, F.H. Estupiñán, P. Zambrano R, J. A. Cabral M, C. Barrios, F. Almeraya Calderón *Int. J. Electrochem. Sci.* 11(2016) 1080.
25. S. Kou, "Welding Metallurgy", John Wiley & Sons, Inc. (2003) Hoboken, New Jersey USA.
26. P. Marcus and J. Oudar, "Corrosion Mechanisms in Theory and Practice", Marcel Dekker, Inc. (2002) New York, USA.
27. T. C. Scalise, M. C. L. D. Oliveira, I. J. Sayeg and R. A. Antunes, *J. of Mater Eng Perform.* 23 (2014) 2164.
28. J. H. Park, H. S. Seo and K. Y. Kim, *J Electrochem. Soc.* 168 (2015) C412.
29. M. V. Venkatesan, N. Murugan, S. Sam and S. K. Albert, *Trans Indian Inst Met.* 67 (2014) 375.
30. M. Alizadeh-Sh, S. P. H. Marashi and M. Pouranvari, *Mater Design* 56 (2014) 258.
31. T. Balusamy, S. Kumar, T.S.N. Sankara Narayanan, *Corros. Sci.* 52 (2010) 3826.